Inorganica Chimica Acta 374 (2011) 261–268

Contents lists available at ScienceDirect

Inorganica Chimica Acta

journal homepage: www.elsevier.com/locate/ica

Mononuclear copper(I) complexes of *O*-*t*-butyl-1,1-dithiooxalate and of *O*-*t*-butyl-1-perthio-1-thiooxalate

David F. Zigler [a], Elisa Tordin [b], Guang Wu [a], Alexei Iretskii [c], Elena Cariati [b], Peter C. Ford [a,*]

[a] *Department of Chemistry and Biochemistry, University of California-Santa Barbara, Santa Barbara, CA 93106-9510, USA*
[b] *Dipatimento di Chimica Inorganica Metallorganica e Analitica "Lamberto Malatesta", Università di Milano and Centro CNR-ISTM, Via Venezian 21, 20133 Milano, Italy*
[c] *Department of Chemistry and Environmental Sciences, Lake Superior State University, Sault Ste. Marie, MI 49783, USA*

ARTICLE INFO

Article history:
Available online 19 February 2011

Dedicated to Prof. W. Kaim.

Keywords:
Copper complexes
X-ray crystal structure
Thiol ligands

ABSTRACT

Described are the syntheses and structures of a phosphonium salt of the anionic ligand *O*-*t*-butyl-1,1-dithiooxalate, $[PPh_3Bz][i\text{-dto}^tBu]$ ($[PPh_3Bz][\mathbf{1}]$), and of two Cu(I) complexes of this anion, $Cu(PPh_3)_2(\eta^2\text{-}i\text{-dto}^tBu)$ (**2**) and $Cu(dmp)(PPh_3)(\eta^1\text{-}i\text{-dto}^tBu)$ (**3**, dmp = 2,9-dimethyl-1,10-phenanthroline). In addition, it was found that the reaction of $CuBr_2$ with $i\text{-dto}^tBu^-$ gives a *O*-*t*-butyl-1-perthio-1-thiooxalato complex of copper(I), $[BzPh_3P][Cu(Br)(S\text{-}i\text{-dto}^tBu)]$ ($[BzPh_3P][\mathbf{4}]$), where $[S\text{-}i\text{-dto}^tBu]^-$ is a disulfide-containing anionic ligand. The electronic structure and absorption spectrum of this species were investigated by time dependent DFT methods.

1. Introduction

Interest in exploring the reactions of photochemically non-innocent ligands [1] has led us to initiate studies of complexes based on derivatives of 1,1-dithiooxalate [2–7], specifically *O*-*t*-butyl-1,1-dithiooxalate, $[i\text{-dto}^tBu]^-$ (**1**) (Fig. 1). Described here are the preparations and structures of two copper(I) complexes of **1**, $Cu(PPh_3)_2(i\text{-dto}^tBu)$ (**2**) and $Cu(dmp)(PPh_3)(\eta^1\text{-}i\text{-dto}^tBu)$ (**3**, dmp = 2,9-dimethyl-1,10-phenanthroline). In the course of preparing such complexes, we found that the reaction of **1** with $CuBr_2$ gives a complex with a bidentate perthiocarboxylato ligand, and the structure and electronic properties of this new complex salt $[BzPh_3P][Cu(Br)(S\text{-}i\text{-dto}^tBu)]$ ($[BzPh_3P][\mathbf{4}]$, $S\text{-}i\text{-dto}^tBu^-$ = *O*-*t*-butyl-1-perthio-1-thiooxalato) are described.

2. Experimental

2.1. $[BzPh_3P][i\text{-dto}^tBu]$ ($[BzPh_3P][\mathbf{1}]$)

The anionic ester *O*-*t*-butyl-1,1-dithiooxalate ($i\text{-dto}^tBu^-$, **1**) was synthesized as its benzyltriphenylphosphonium salt using a procedure adapted from Strauch et al. [2]. Sulfur (1.92 g, 60.0 mmol) and 12.5 mL of triethylamine (90.0 mmol) was stirred in 30 mL of deoxygenated dimethylformamide for ca. 50 min. *O*-*t*-Butyl-2-chloroacetate (4.52 g, 30.0 mmol) was added in one portion to the dark green solution, turning it deep orange. The temperature of the reaction was kept at 20–30 °C using a water bath and adding ice as needed over 2 h. Precipitated $[NHEt_3]Cl$ was separated by vacuum filtration and rinsed with 2× 5 mL of DMF. The filtrate was added to 11.7 g of $[BzPh_3P]Cl$ (30.0 mmol) dissolved in 30 mL of MeOH. Crude $[BzPh_3P][\mathbf{1}]$ was precipitated by slow addition of 80 mL of water over ca. 50 min. Following filtration, excess DMF and water were removed by suspending the crude plug of $[BzPh_3P][\mathbf{1}]$ in 200 mL of diethyl ether and filtering. The salt $[BzPh_3P][\mathbf{1}]$, recrystallized twice from $CH_2Cl_2/i\text{-PrOH}$, was isolated as 5.24 g of dark orange crystals (9.87 mmol, 33% yield). $[BzPh_3P][\mathbf{1}]$ is soluble in CH_2Cl_2, and $CHCl_3$ and is somewhat soluble in MeOH, EtOH and in mixed solvents (e.g., 1:2 CH_2Cl_2/EtOH). ^1H NMR (CD_2Cl_2): $\delta = 6.98–7.82$ (20H, m, Ar), 4.89 (2H, d, $^2J_{P–H} = 14.2$), 1.41 (9H, s) ppm. ^{13}C NMR (CD_2Cl_2): $\delta = 246.3$ (CS_2), 170.4 (CO_2), 127–136 (multi. C_{Ar}), 117.6 ($P–CH_2–Ph$, $^1J_{CP} = 88$ Hz), 80.1 (C_{tBu}), 28.1 (Me_{tBu}) ppm. UV–Vis (MeOH): $\lambda_{max} = 343$ (14 600 $M^{-1}\,cm^{-1}$), 267 nm (4280 $M^{-1}\,cm^{-1}$). FTIR (KBr): $\nu = 2986$(w), 2921(w), 2881(w), 3051(w), 3017(w), 1691(C=O, vs), 1586(m), 1483(m), 1455(m), 1438(s), 1366(m), 1267(m), 1253(m), 1168(s), 1154(m), 1110(s), 1043(vs), 1001(m), 995(m), 850(m), 835(m), 803(m), 780(m), 752(m), 747(s), 718(m), 697(s), 689(s), 578(m), 512(s), 505(s), 495(s) cm^{-1}. See Supporting information for key spectra.

X-ray quality single crystals were grown by slow diffusion of *i*-PrOH into a concentrated CH_2Cl_2 solution of $[BzPh_3P][i\text{-dto}^tBu]$ at −20 °C.

2.2. $Cu(PPh_3)_2(i\text{-dto}^tBu)$ (**2**)

This was prepared following procedures adapted from Strauch et al. [2]. In a 100 mL beaker, 0.89 g of $CuCl(PPh_3)_3$ (1.0 mmol)

---

[*] Corresponding author.
E-mail address: ford@chem.ucsb.edu (P.C. Ford).

0020-1693/$ - see front matter © 2011 Elsevier B.V. All rights reserved.
doi:10.1016/j.ica.2011.02.037

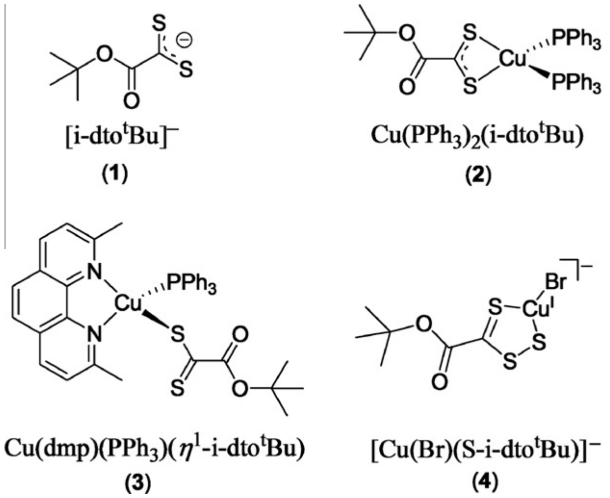

$[\text{i-dto}^t\text{Bu}]^-$
(1)

$Cu(PPh_3)_2(\text{i-dto}^t\text{Bu})$
(2)

$Cu(dmp)(PPh_3)(\eta^1\text{-i-dto}^t\text{Bu})$
(3)

$[Cu(Br)(\text{S-i-dto}^t\text{Bu})]^-$
(4)

Fig. 1. Ligand and complexes described in this study.

was dissolved in 20 mL of CH_2Cl_2 and 0.53 g of $[BzPh_3P]$[**1**] (1.0 mmol) in 30 mL of CH_2Cl_2 was added dropwise over 5 min. The dark reaction mixture was covered with a watch glass and stirred in the dark for 1 h. The solvent was removed under reduced pressure and the residue was recrystallized twice from CH_2Cl_2/*i*-PrOH at −20 °C. Pale brown needles of **2** crumbled upon drying to give 0.64 g (0.84 mmol, 84%) of brown powder. ^1H NMR (CD_2Cl_2): $\delta = 7.1–7.4$ (30H, m), 1.43 ppm (9H, s). FTIR (KBr): $\nu = 2982$(w), 2935(w), 3054(w), 1703(C=O, vs), 1478(s), 1432(vs), 1389(m), 1365(m), 1253(b,vs), 1156(b,vs), 1092(s), 1077(s), 1052(s), 1018(s), 997(m), 843(m), 811(m), 744(vs), 694(vs), 527(m), 516(s), 501(s) cm^{-1}. UV–Vis (CH_2Cl_2): λ_{max} (ε) = 400 (sh, 3000 M^{-1} cm^{-1}) 364 (5230 M^{-1} cm^{-1}), 265 nm (23 100 M^{-1} cm^{-1}). See Supporting information for key spectra.

X-ray quality crystals of $Cu(PPh_3)_2$(*i*-dto^{t}Bu) were isolated after slow diffusion of *i*-PrOH into a concentrated solution of **2** in CH_2Cl_2 at room temperature.

2.3. $Cu(dmp)(PPh_3)(\eta^1\text{-i-dto}^t\text{Bu})$ (**3**)

A deoxygenated solution of **2** (0.20 g, 0.26 mmol) in minimal CH_2Cl_2 was charged with 0.055 g of 2,9-dimethyl-1,10-phenanthroline (0.26 mmol), also in a minimal amount of deaerated CH_2Cl_2. Following 3 days at 5 °C, most of the solvent was removed under flowing argon. Diethyl ether was layered on the reaction concentrate to give small orange crystals after 3 days at −20 °C. Following filtration and drying, the crystals crumbled giving 0.11 g of air-sensitive, bright yellow microcrystals (0.16 mmol, 62% yield). Calc. for $CuC_{38}H_{36}N_2O_2PS_2$: C, 64.2; H, 5.10; N, 3.94. Found: C, 63.6; H, 5.13; N, 4.03%. FTIR (KBr): $\nu = 2981$(w), 2931(w), 3056(w), 3005(w), 1695(C=O, s), 1652(m), 1616(m), 1588(m), 1558(m), 1538(m), 1506(m), 1498(m), 1478(w), 1456(m), 1434(s), 1366(s), 1275(b,s), 1254(b,s), 1165(b,s), 1151(m), 1092(m), 1066(s), 1038(m), 988(s), 860(m), 842(m), 742(s), 731(m), 695(s), 522(s), 503(m), 491(m) cm^{-1}. See Supporting information for key spectra.

X-ray quality crystals of $Cu(dmp)(PPh_3)(\eta^1$-*i*-dto^{t}Bu)·CH_2Cl_2 were isolated after slow diffusion of Et_2O into the reaction mixture at −20 °C. The crystals readily lost the CH_2Cl_2 of crystallization, so care was made to maintain the crystals at low temperature (150 ± 2 K).

2.4. $[BzPh_3P][Cu(Br)(\text{S-i-dto}^t\text{Bu})]\cdot0.5THF$ ($[BzPh_3P]$[**4**]·0.5THF)

Under argon flow a solution of 0.40 g of $[BzPh_3P]$[**1**] (0.75 mmol, 2.1 equiv) in ca. 10 mL dichloromethane was added slowly to a stirring deaerated solution of 0.080 g of $CuBr_2$ (0.36 mmol) in a minimal amount of water (ca. 3 mL). The aqueous phase was removed after 30 min of stirring and the organic layer was concentrated in vacuo. The resulting violet solid was washed with 3 × 1 mL of THF and gravity filtered through a glass wool packed Pasture pipette to extract the complex salt. Narrow red plates obtained from slow diffusion of diethyl ether into the combined THF washings were filtered, washed with Et_2O and recrystallized to give 0.16 g of $[BzPh_3P]$[**4**]·0.5THF (0.21 mmol, 60% yield). Calc. for $CuC_{33}H_{35}BrO_{2.5}PS_3$: C, 53.4; H, 4.75. Found: C, 53.5; H, 4.45%. ESI(−)-MS (CH_3CN or THF): *m/z* (rel. peak height) = 350.81(77), 351.83(9.6), 352.81(100), 353.81(13), 354.81(51), 355.83(5.7), 356.82(7.1); theoretical for $CuC_6H_9BrO_2S_3$: *m/z* (rel. peak height) = 350.82(64), 351.83(4.3), 352.82(100), 353.83(6.1), 354.82(41), 355.82(3.6), 356.82(4.1). FTIR (KBr): $\nu = 2980$(m), 2918(m), 2836 (m), 3056(w), 1717(b,s), 1586(m), 1492(m), 1482(m), 1454(m), 1436(s), 1392(m), 1368(m), 1255(b,s), 1151(b,s), 1111(s), 1074(b,s), 1031(w), 996(m), 921(w), 866(w), 836(m), 787(m), 743(m), 717(m), 700(m), 688(s), 582(m), 558(m), 510(s), 499(m), 446(w). UV–Vis (THF): λ_{max} (ε) = 358 (3730 M^{-1} cm^{-1}), 512 (3420 M^{-1} cm^{-1}), 720 (shoulder, 27 M^{-1} cm^{-1}) nm. See Supporting information for key spectra.

X-ray quality crystals were obtained from slow vapor diffusion of Et_2O into a THF solution of $[BzPh_3P]$[**4**] at room temperature.

2.5. Instruments

Electronic absorption spectra were measured in spectroscopic grade solvent using a Varian-Cary UV-2401PC double beam UV–Vis spectrophotometer. Infrared spectra were recorded for samples in KBr pellets using a Mattson FTIR at 2 cm^{-1} resolution and averaging 32 scans. NMR spectra (^1H- and ^{13}C) were measured in deuterated solvent on either a 200 MHz Varian MERCURY Vx or a 500 MHz Varian UNITY INNOVA instrument. Mass spectrometry was performed either with a Micromass Q-ToF using a standard electrospray source (acetonitrile) or with a modified Q-ToF instrument using a nanospray source (THF) [8]. Source, cone and impact chamber potentials were optimized to decrease ion fragmentation. Theoretical mass spectra were determined for specific ions using the isotopic distribution calculator in the ChemDraw Ultra Suite of programs.

2.6. X-ray crystallography

The solid state structures of the new series of molecules were determined using standard procedures. A Bruker 3-axis platform diffractometer was used to measure reflections for crystals of $[BzPh_3P]$[*i*-dto^{t}Bu], $Cu(PPh_3)_2$(*i*-dto^{t}Bu), $Cu(dmp)(PPh_3)(\eta^1$-*i*-dto^{t}Bu) and $[BzPh_3P]$[Cu(Br)(S-*i*-dto^{t}Bu] using Mo Kα radiation selected with a graphite monochromator ($\lambda = 0.71070$ Å) and detected via SMART 1000 CCD. With the exception of $[BzPh_3P]$[**1**] (293 ± 2 K), structures were measured at 150 ± 2 K.

Single crystals of the new species were obtained as follows: $[BzPh_3P]$[**1**] crystallized from CH_2Cl_2/*i*-PrOH as orange blocks in the orthorhombic space group *Fdd*2. Orange plates of **2** in the triclinic space group $P\bar{1}$ were obtained by layering *i*-PrOH on a concentrated CH_2Cl_2 solution and allowing the CH_2Cl_2 to evaporate slowly at room temperature. **3**·CH_2Cl_2 crystallized upon slow diffusion of Et_2O into a CH_2Cl_2 solution as yellow blocks in the monoclinic space group $P2_1/c$. $[BzPh_3P]$[**4**]·0.5THF was obtained by vapor diffusion of Et_2O into a room temperature solution in THF to give red plates in the monoclinic space group $P2_1k$ crystal structures were solved with SHELXS-97 using experimental parameters listed in Table 1 and refined using SHELXL-97 [9]. Hydrogens were empirically placed using a constrained geometric arrangement based on energy minimized distances.

Table 1
Experimental parameters and crystallographic results for the series of *O-t*-butyl-1,1-dithiooxalate species.

	$[BzPh_3P][\mathbf{1}]$	**2**	$\mathbf{3}\cdot CH_2Cl_2$	$[BzPh_3P][\mathbf{4}]\cdot 0.5THF$
Formula	$C_{31}H_{31}O_2PS_2$	$C_{42}H_{39}CuO_2P_2S_2$	$C_{39}H_{38}Cl_2CuN_2O_2PS_2$	$C_{33}H_{35}BrCuO_{2.50}PS_3$
F_w	530.65	765.33	796.24	742.21
Symmetry	orthorhombic	triclinic	monoclinic	monoclinic
Morphology	orange block	orange plate	yellow block	red plate
Crystal dimension (mm)	0.3 × 0.3 × 0.2	0.3 × 0.15 × 0.08	0.2 × 0.2 × 0.1	0.35 × 0.1 × 0.07
a (Å)	52.853(3)	10.262(2)	16.712(5)	10.108(2)
b (Å)	13.0849(8)	13.096(3)	19.210(6)	9.2736(19)
c (Å)	16.6948(10)	14.625(3)	11.621(4)	38.513(8)
α (°)	90	88.430(3)	90.00	90.00
β (°)	90	76.123(3)	91.136(5)	95.567(3)
γ (°)	90	76.584(3)	90.00	90.00
Unit-cell volume (Å^3)	11545.8(12)	1855.2(6)	3730(2)	3592.9(13)
T (K)	293(2)	150(2)	150(2)	150(2)
Space group	$Fdd2$	$P\bar{1}$	$P2_1$/i	$P2_1/c$
Z	16	2	4	4
μ (cm^{-1})	2.65	8.23	9.21	19.67
Total reflections	16 494	13 778	30 074	28 745
Unique reflections	5490	7026	7570	6097
Reflections $[I > 2\sigma(I)]$	4392	4777	5484	4548
S[a]	1.18[b]	1.029[b]	1.496[b]	1.587[c]
R[a]	0.0460[b]	0.0476[b]	0.0524[b]	0.0854[c]
$R(w)$[a]	0.1036[b]	0.1000[b]	0.1335[b]	0.2032[c]

[a] Refinement of F^2 against all reflections. The weighted *R*-factor $R(w)$ and goodness of fit S are based on F^2, conventional *R*-factors R are based on F, with F set to zero for negative F^2. The threshold expression of $F^2 > 2\sigma(F^2)$ is used only for calculating *R*-factors, etc. and is not relevant to the choice of reflections for refinement.

[b] Weighting factor $(w) = [s^2(F_o^2) + (0.0500P)^2 + 0.0000P]^{-1}$, where $P = ((F_o^2 + 2F_c^2)/3$.

[c] Weighting factor $(w) = [s^2((F_o^2) + (0.0686P)^2 + 0.0000P]^{-1}$, where $P = (F_o^2 + 2F_c^2)/3$.

2.7. DFT calculations

Density functional theory calculations were performed on the anion Cu(Br)(S-*i*-dto^{t}Bu)$^-$ in an effort to understand the observed electronic properties. For comparisons, geometries and Cu-local ionization energies (E_{LIP}) were calculated using the B3LYP functional with the 6-31G* basis set for **4** and several other tricoordinate models. The 12 lowest energy electronic excited states of **4** were calculated with SPARTAN '08 using time-dependent (TD) DFT, also at the B3LYP/6-31G* level [10].

3. Results and discussion

3.1. Syntheses

The anionic ligand *O-t*-butyl-1,1-dithiooxalate (**1**, *i*-dto^{t}Bu$^-$) was prepared by the reaction of sulfur with *t*-butyl-2-chloroacetate following procedures adapted from Strauch et al. [2] and isolated as the benzyltriphenylphosphonium salt. This salt was used as the source of the anionic ligand **1** in the subsequent reactions. Reaction of $[BzPh_3P][\mathbf{1}]$ with $CuCl(PPh_3)_3$ gave $Cu(PPh_3)_2$(*i*-dto^{t}Bu) (**2**) with a bidentate dithiocarboxylate group in agreement with the earlier synthesis [2] of the analogous methyl complex $Cu(PPh_3)_2$(*i*-dtoMe). Reaction of **2** with 1 equiv of 1,10-dimethyl-2,9-phenanthroline led to displacement of one PPh_3 and formation of the monodentate dithiolcarboxylato complex Cu(dmp)(PPh_3)(η^1-*i*-dto^{t}Bu) (**3**).

The room temperature biphasic reaction under argon of aqueous $CuBr_2$ with 2.1 equiv of $[BzPh_3P]$[*i*-dto^{t}Bu] in CH_2Cl_2 led to formation not of a complex of **1** but to a complex of the unexpected perthiocarboxylato ligand S-*i*-dto^{t}Bu$^-$. The crude $[BzPh_3P]$[Cu(Br)(S-*i*-dto^{t}Bu)] salt ($[BzPh_3P][\mathbf{4}]$) was isolated and then recrystallized by slow diffusion of diethyl ether into a THF solution and separating the dark red needles from a white amorphous material, probably $[BzPh_3P]Br$.

The formation of **4** involves oxidation of the ligand **1** and reduction of Cu(II) to Cu(I) with the extra sulfur of the perthioligand coming from the excess **1**. Scheme 1 suggests a possible pathway by which this might occur. Interestingly, attempts to prepare **4** using $CuSO_4$ or $Cu(OAc)_2$ did not result in analogous products suggesting that the bromide plays a role, perhaps by stabilizing the product.

3.2. Structures determined by X-ray crystallography

The crystal structure of $[BzPh_3P]$[*i*-dto^{t}Bu)] (Fig. 2) is the first reported for an uncoordinated *O*-alkyl-1,1-dithiooxalate anion.

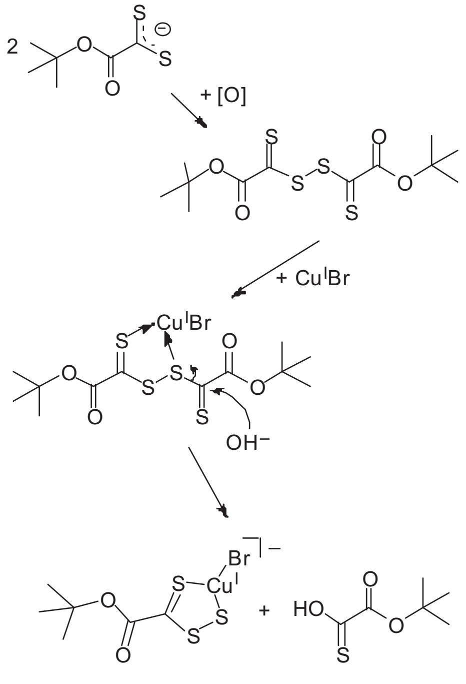

Scheme 1. Speculative pathway for the formation of **4** from $CuBr_2$ and **1**.

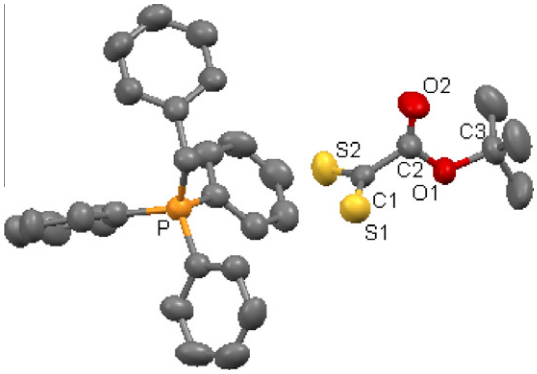

Fig. 2. Crystal structure of $[BzPh_3P][\mathbf{1}]$ showing 50% thermal ellipsoids, $T = 293$ K. Hydrogens omitted for clarity.

The C–S bond distances of 1.659(3) and 1.666(3) Å in **1** are slightly shorter than those reported for the 1,1-dithiooxalate dianion in $Cs_2[i\text{-dto}]\cdot CsCl\cdot H_2O$, C–S = 1.68(1) Å [12]. As expected, the C–O bond lengths within the ester, 1.331(4) and 1.203(4) Å, are consistent with respective single and double bonds. The C–C distance of 1.519(4) Å also is consistent with a single bond. The torsion angle between S–C–S and O–C–O planes is 89.4(3)°. The S–C–S angle is 129.11(18)°, and is close the value 128.6(8)° reported for the *i*-dto^{2-} anion [12]. Other selected properties are summarized in Table 2.

The structure of $Cu(PPh_3)_2(i\text{-dto}^tBu)$ (**2**) (Fig. 3), is similar to that of the previously reported methyl ester analog $Cu(PPh_3)_2(i\text{-dtoMe})$ with nearly the same C–S distances, 1.682(4) and 1.663(4) Å [2]. The Cu–S distances, 2.4928(11) and 2.3694(11) Å, are longer than for less sterically encumbered systems [13]. Contrary to $[BzPh_3P][\mathbf{1}]$ and the methyl analog, the 1,1-dithiooxalate backbone is nearly coplanar, with a torsion angle of only 10.9(5)°. The C–C distance of 1.528(5) Å is again consistent with a single bond. These and other data are summarized in Table 3.

Table 2
Selected interatomic distances for $[BzPh_3P][i\text{-dto}^tBu]$.

Atom	Bond length (Å)[a]	Atoms	Bond angle (°)[a]
C_1–S_1	1.666(3)	S_1–C_1–S_2	129.11(18)
C_1–S_2	1.659(3)	S_1–C_1–C_2	116.2(2)
C_1–C_2	1.519(4)	O_2–C_2–C_1	123.7(3)
C_2–O_1	1.331(4)	O_2–C_2–O_1	125.5(3)
C_2–O_2	1.203(4)		
O_1–C_3	1.478(3)		Torsion angle (°)[a]
C_3–C_4	1.512(5)	S_2–C_1–C_2–O_2	89.4(3)

[a] Value in parentheses is error in last significant digit.

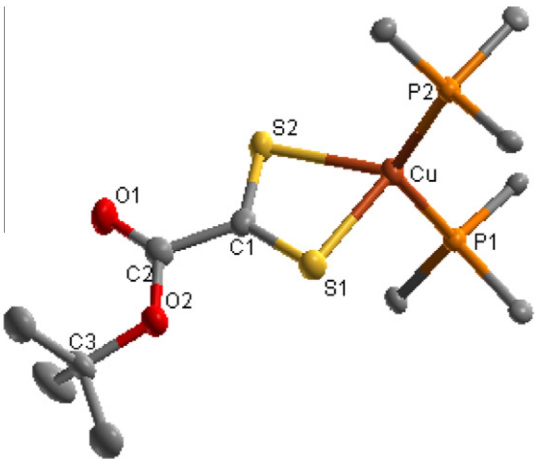

Fig. 3. Crystal structure of **2** (50% thermal ellipsoids) at 150 K. Hydrogens and phenyl rings omitted for clarity.

Table 3
Selected structural details for $Cu(PPh_3)_2(i\text{-dto}^tBu)$.

Atom	Bond length (Å)[a]	Atoms	Bond angle (°)[a]
Cu–P_1	2.2727(10)	S_1–Cu–S_2	73.75(3)
Cu–P_2	2.2685(10)	P_1–Cu–P_2	125.98(4)
Cu–S_1	2.4928(11)	S_2–Cu–P_2	111.86(4)
Cu–S_2	2.3694(11)	S_1–Cu–P_2	107.00(4)
C_1–S_1	1.682(4)	S_1–C_1–S_2	121.6(3)
C_1–S_2	1.663(4)	C_2–C_1–S_2	117.5(3)
C_1–C_2	1.528(5)	C_1–C_2–O_2	111.5(3)
C_2–O_1	1.213(4)		
C_2–O_2	1.337(4)		Torsion angle (°)[a]
O_2–C_3	1.485(4)	O_1–C_2–C_1–S_2	10.9(5)

[a] Value in parentheses is error in last significant digit.

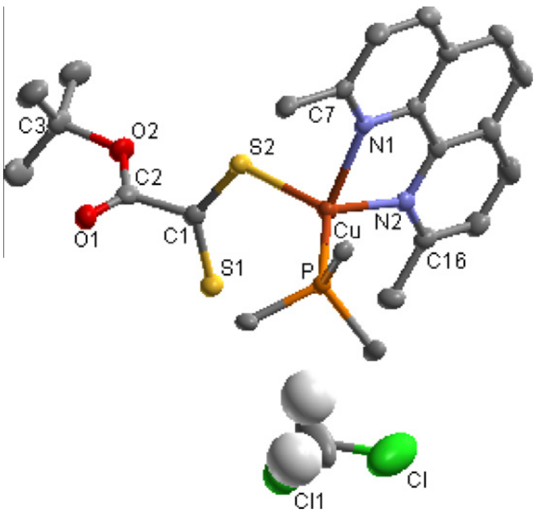

Fig. 4. Crystal structure of $\mathbf{3}\cdot CH_2Cl_2$ showing 50% thermal ellipsoids ($T = 150$ K). Hydrogens and phenyl rings omitted for clarity.

Table 4
Selected interatomic distances for $Cu(dmp)(PPh_3)(\eta^1\text{-}i\text{-dto}^tBu)]\cdot CH_2Cl_2$.

Atom	Bond length (Å)[a]	Atoms	Bond angle (°)[a]
Cu–P	2.2253(11)	N_1–Cu–N_2	80.03(10)
Cu–S_2	2.3096(11)	S_2–Cu–P	122.58(4)
Cu···S_1	3.771	S_2–Cu–N_2	111.97(8)
Cu–N_1	2.133(3)	S_1–C_1–S_2	128.9(2)
Cu–N_2	2.084(3)	C_1–S_2–Cu	113.00(12)
C_1–S_1	1.656(3)	C_2–C_1–S_2	114.6(2)
C_1–S_2	1.686(3)	C_1–C_2–O_2	111.6(3)
C_1–C_2	1.518(5)		
C_2–O_1	1.203(4)		Torsion angle (°)[a]
C_2–O_2	1.329(4)	C_1–S_2–Cu–P	61.28(14)
O_2–C_3	1.505(4)	O_1–C_2–C_1–S_2	106.0(3)

[a] Value in parentheses is error in last significant digit.

The structure of $Cu(dmp)(PPh_3)(\eta^1\text{-}i\text{-dto}^tBu)$ (**3**) clearly shows the monodentate coordination of the *i*-dto^{t}Bu$^-$ anion (Fig. 4 and Table 4). Surprisingly, the C–S distances 1.656(3) and 1.686(3) Å for the C=S and C–S, respectively, are only modestly different than those seen for the η^2 precursor **2**. However, the Cu–S distance at 2.3096(11) Å is considerably shorter than in **2** perhaps as the result of backbonding from Cu(I) into the dmp acceptor that would make

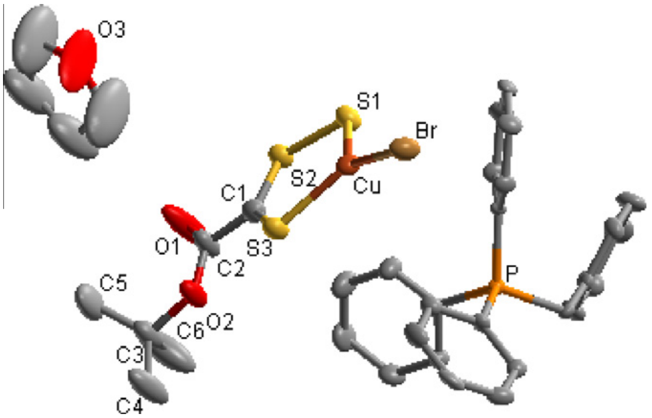

Fig. 5. Crystal structure of [BzPh$_3$P][**4**]·0.5THF showing 50% thermal ellipsoids, *T* = 150 K. Hydrogens omitted for clarity.

Table 5
Selected interatomic distances for [BzPh$_3$P][**4**]·0.5THF.

Atom	Bond length (Å)[a]	Atoms	Bond angle (°)[a]
Cu–Br	2.2869(14)	S_1–Cu–S_3	99.33(9)
Cu–S_1	2.216(2)	S_1–Cu–Br	129.66(8)
Cu–S_3	2.212(2)	S_3–Cu–Br	130.96(8)
S_1–S_2	1.985(3)	S_3–C_1–S_2	126.9(5)
C_1–S_2	1.700(8)	C_1–S_2–S_1	108.6(3)
C_1–S_3	1.657(8)	C_2–C_1–S_2	109.5(6)
C_1–C_2	1.494(12)	C_2–C_1–S_3	123.6(6)
C_2–O_1	1.195(10)		
C_2–O_2	1.304(10)		Torsion angle (°)[a]
Cu···Cu	8.785	C_1–S_2–S_1–Cu	3.7(3)
(nearest)		O_1–C_2–C_1–S_2	11.6(13)

[a] Value in parentheses is error in last significant digit.

the copper center more electro-positive. The Cu–P distance is also shorter, 2.2253(11) Å. The torsion angle about the 1,1-dithiooxalate C–C backbone is 106.0(3)° and the bond distance of 1.518(5) Å indicates this to be a C–C single bond.

The crystal structure of the mononuclear perthiocarboxylate complex [BzPh$_3$P][**4**]·0.5THF is presented in Fig. 5, with selected structural properties listed in Table 5. Remarkably, this structure displays a 3-coordinate Cu(I). Around the CuSSC=S ring, the measured bond distances are, respectively, 2.216(2), 1.985(3), 1.700(8) and 1.657(8) Å with a 2.212(2) Å Cu–S$_{(S=C)}$ bond closing the ring. The C–C distance within the dithiooxalate backbone, though slightly shorter than the preceding systems at 1.494(12) Å, is reasonable for a single bond. The torsion angle between CS$_2$ and CO$_2$ moieties was measured at 11.6(13)°. The CuSSC=S ring, bromide and ester carbon are all coplanar, deviating by no more than 3.5° from planarity. The S–Cu–S angle is 99.33(9)° with the bromide centered between the bound S atoms; S–Cu–Br $\approx$ 130°. The distorted trigonal planar coordination environment of Cu(I) is evident even in the packing diagram (Fig. 6) which shows no other ligands, including cations and solvent, within a normal distance for coordination. The shortest distance between any two copper atoms was 8.785 Å and the closest non-bonded atoms, phenyl hydrogens, are 2.96–3.90 Å distant.

The structure of the chelating perthiolcarboxylato ligand in [BzPh$_3$P][**4**] differs from other metal-perthio-thionyl systems as indicated by representative structures summarized in Table 6 [3,4,7,15–23]. As might be expected for metals with differing radii, the M–S bond lengths vary from 2.13 to 2.35 Å. For most of the complexes the M–S$_{(S=C)}$ and M–S$_{(S-S)}$ bond lengths are similar, suggesting equivalent metal/sulfur interactions. Octahedral systems such as [Fe(S$_3$C-PhMe)(S$_2$CPhMe)$_2$], [15] [M(S$_3$CAr)$_2$(S$_2$CAr)] (M = Tc, Re) [16,17] and clusters [21–23] have longer relative M–S$_{(S=C)}$ bonds. On par with other planar systems, [BzPh$_3$P][**4**] has nearly identical Cu–S bonds, 2.212(2) and 2.216(2) Å. These short Cu–S bonds are comparable to [CuCl(dptu)$_2$], dptu = *N,N′*-diphenylthiourea (Cu–S = 2.22 Å) [13], and support a strong covalent interaction between copper and sulfur. These Cu–S bonds are considerably shorter than seen for **2** (2.3694(11) and 2.4928 Å) or **3** (2.3096(11) Å). The C–S bond lengths vary widely between MSSC=S ring systems, with little indication of the impact of metal *d*-electron count or thionyl carbon substituent effects. Generally the C=S bond is shorter than the carbon bond to the disulfide sulfur, aligning with a difference in bond order. The d^{10} complexes [Zn(S$_3$CPh-^{i}Pr)$_2$] [20] and [BzPh$_3$P][**4**] exhibit the largest disparity in C–S bonds with 1.6641(6), 1.711(6) Å and 1.657(8), 1.700(8) Å, respectively.

The unusually short disulfide bond length in **4** can be rationalized by considering the electronic influences of the thionyl carbon and Cu(I) center in this cyclic structure. Unhindered disulfides

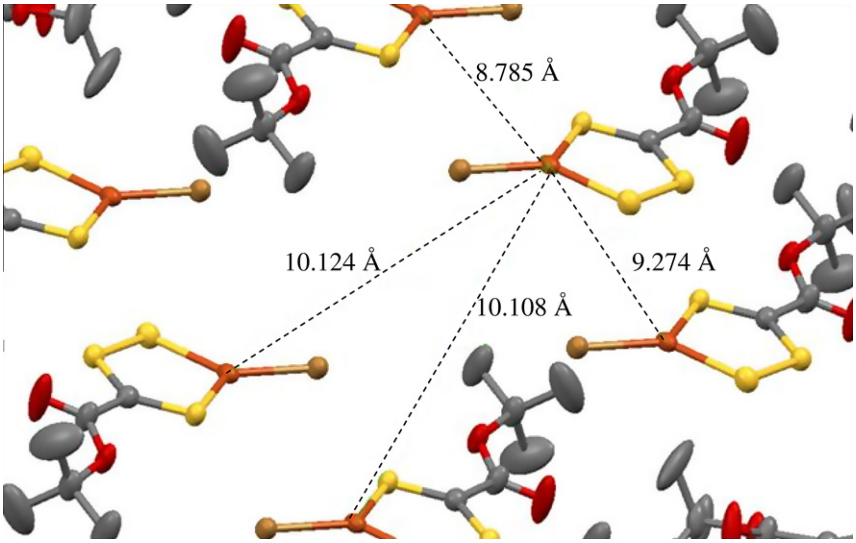

Fig. 6. Crystal packing illustration of [BzPh$_3$P][**4**]·0.5THF showing the distances between the central copper and its closest four neighbors (Å). Cation, solvent and hydrogens have been omitted for clarity.

Table 6
Selected structural values from five-membered rings formed by a transition metal and chelated perthioligands.

Molecule perthioligand[a]	Atom distances (Å)[b]						Ref.
	C═S	C–S	S–S	M–S═	M–S–	C–R	
Organic analogs							
MDCT	1.627[c]	1.747	2.047				[14]
MePhC(S)SSC(S)PhMe	1.61	1.78	2.023(6)			1.52	[11]
Monometallic complexes							
Fe(S-dtt)(dtt)$_2$[d]	1.692(2)	1.705(3)	2.086(8)	2.240(2)	2.183(4)	1.468(1)	[15]
Re(S-dtb)$_2$(dtb)	1.647(7), 1.656(7)	1.689(6), 1.676(7)	2.102(3), 2.068(3)	2.320[e]	2.199[e]	1.457(9), 1.467(8)	[16]
Tc(S-dtb)$_2$(dtb)	1.667, 1.672	1.686, 1.703	2.075, 2.098	2.354, 2.348	2.227, 2.230	1.478, 1.472	[17]
ReS(S$_4$)(S$_3$CMe$_2$)[i]	1.820(21)	1.816(21)	2.061(9)	2.285(6)	2.274(6)	1.519(30), 1.549(33)	[18]
[Ph$_4$P][Ni(S-*i*-dto-OMe) (*i*-dto-OMeacac)]	1.67(2)	1.67(2)	2.013(8)	2.124(6)	2.148(6)	1.49(3)	[3]
[Ph$_4$P][Ni(S-*i*-dto-OMe)(S$_2$CC(CN)$_2$)]	1.689(8)	1.669(10)	2.011(4)	2.129(3)	2.133(3)	1.467	[4]
Pt(S$_3$CMe)$_2$	1.667(7)	1.695(6)	2.045(2)	2.2715(14)	2.2959(16)	1.498(9)	[7]
Ni(S$_3$CMe)$_2$	1.667(3)	1.668(3)	2.0322(12)	2.1579(8)	2.1623(4)	1.496(4)	[19]
Ni(S$_3$CMe)(S$_2$CMe)	1.681(6)	1.638(6)	2.027(2)	2.1331(18)	2.1225(18)	1.506(8)	[7]
Ni(S$_2$CPh-^{i}Pr)(S$_3$CPh-^{i}Pr)	1.678(9)	1.699(8)	2.016(4)	2.138(5)	2.130(3)	1.385(6)	[20]
Zn(S$_3$CPh-^{i}Pr)$_2$	1.664(6)	1.711(6)	2.008(4)	2.327(2)	2.316(3)	1.48(1)	[20]
Cu(Br)(S-*i*-dto-O^{t}Bu)	1.657(8)	1.700(8)	1.985(3)	2.212(2)	2.216(2)	1.494(12)	t.w.
Bridged multimetallic complexes[f]							
[Os$_2$(μ-S-dtcEt$_2$)$_2$(dtcEt$_2$)$_3$] [BPh$_4$][g]	1.71(4), 1.76(3)	1.66(4), 1.76(3)	2.05(2), 2.13(1)	2.39(1), 2.36(1)	2.29(1), 2.29(1)[h]	1.32(5)	[21]
K[Ph$_4$P][Cu$_4$(S-^{t}BuDED)$_3$][g]	1.716(9)	1.766(10)	2.076(4)	2.272(3)[h]	2.211(3)[h]	1.392(13)	[22]
[Bu$_4$N]$_6$[Cu$_6$(S$_3$CC(CN)$_2$)$_6$]	1.692(6)	1.748(8)	2.053(2)	2.254(2)	2.239(2)[h]	1.408(8)	[23]

[a] MDCT = 4-methyl-1,2-dithia-4-cyclopentene-3-thione; dtt = $^-$S(S)CPhMe; dtb = $^-$S(S)CPh.
[b] From the cyclic arrangement of M–S–S–C═S; C–R is atom nearest to the five-membered ring, nr = not reported.
[c] Exocyclic.
[d] Fe–S–S–C═S ring is folded.
[e] Average of like values (ΔBD < 0.003 Å < RMS).
[f] Situations with bridging perthioligands, only five-member ring dimensions are reported.
[g] Metal–metal bonded clusters.
[h] Sulfur bridges multiple metals.
[i] [S$_3$CMe$_2$]$^{2-}$ is derived from acetone with an sp^3 central carbon and does not have C═S.

typically have a ca. 2.05 Å bond length with a 90° torsion angle around the S–S bond to minimize lone pair repulsive effects [24,25]. Covalently constraining the torsion angle in a ring, such as with trimethylene-1,1-disulfane, generally causes an elongation of the S–S bond to about 2.10 Å and pushes the disulfide π^* to higher energy [25]. Shorter S–S distances are observed with electron withdrawing substituents, for example, the S–S bond of FSSF is only 1.88 Å [26]. An adjacent C═S group may have a similar effect. The S–S bond in the organic model 4-methyl-1,2-dithia-4-cyclopentene-3-thione (MDCT), which has an endocyclic disulfide and an adjacent thionyl carbons is shorter (2.047 Å) than an aliphatic 1,2-dithiolane [14,27]. Acyclic disulfides with adjacent thionyls, RC(═S)SSC(═S)R, also have short S–S bonds (~2.01 Å) [11,28]. While the adjacent thionyl in **4** might have a similar effect on the S–S bond length of the endocyclic disulfide, this should not be sufficient, thus the presence of the Cu(I) center must be the difference. Although Cu(I) is d^{10} with no empty d_π orbitals to stabilize the repulsive effects of sulfur lone pairs, the trigonal planar Cu(I) coordination presents a lower energy 4*p* orbital perpendicular to the CuSSC═S ring with the correct symmetry to interact with the filled disulfide π^* orbital (Fig. 7).

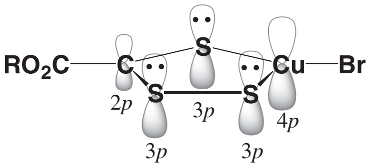

Fig. 7. Illustration of possible *p*-orbital mixing in **4** .

3.3. DFT calculations

Density functional theory computations using the B3LYP functional and the 6-31G* Pople basis set, were employed to probe the electronic properties of **4**. Fig. 8 displays the calculated frontier orbitals for this anion. The HOMO (−4.72 eV) and the LUMO (3.14) are primarily ligand π^* in character with regard to the perthiocarboxylato ligand with the HOMO indicating some contribution from the bromide lone pair perpendicular to the plane of the ring. The HOMO-1 and -2 are largely bromide lone pairs while HOMO-3, -4 and -5 are largely metal ligand bonding orbitals. However, the calculated MO's do not appear to confirm the simple picture proposed in Fig. 7 for Cu(Br)(S-*i*-dto^{t}Bu)$^-$.

3.4. Electronic spectra

The electronic absorption spectra of [BzPh$_3$P][**1**], **2** and [BzPh$_3$P][**4**] are presented in Fig. 9. The solution spectrum for **3** suggested ligand scrambling upon dissolution in CH$_2$Cl$_2$ or THF, consistent with observations made for similar CuX(phen)(PPh$_3$) complexes (phen = 1,10-phenanthroline; X = halide or nitrate) [29–31], thus, is not reported. The spectrum of [BzPh$_3$P][*i*-dto^{t}Bu] in methanol is characterized by a band at $\lambda_{\max}$ = 343 nm (ε = 14 600 M^{-1} cm^{-1}) consistent with the n → π^* of other R—CS$_2^-$ chromophores [32] and a structured band at ~267 nm (4280 M^{-1} cm^{-1}) assigned to $\pi \to \pi^*$ transitions of the aromatic groups on [BzPh$_3$P]$^+$. The spectrum of Cu(PPh$_3$)$_2$(*i*-dto^{t}Bu) in CH$_2$Cl$_2$ displays strong $\pi \to \pi^*$ PPh$_3$ centered bands at ~265 nm (23 100 M^{-1} cm^{-1}) as well as bands at 364 nm (5230 M^{-1} cm^{-1}) and at 400 nm (shoulder, 3000 M^{-1} cm^{-1}) and a low energy tail consistent with the literature [2]. Lastly, the THF solution of

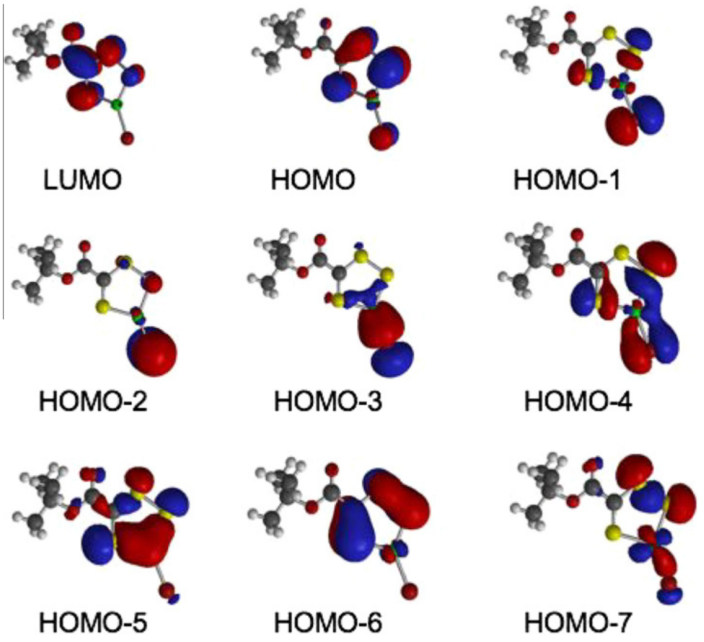

Fig. 8. Pictorial representations of the LUMO, HOMO and HOMO-1 through HOMO-7 for **4** as calculated by DFT at the B3LYP/6-31G* level of theory.

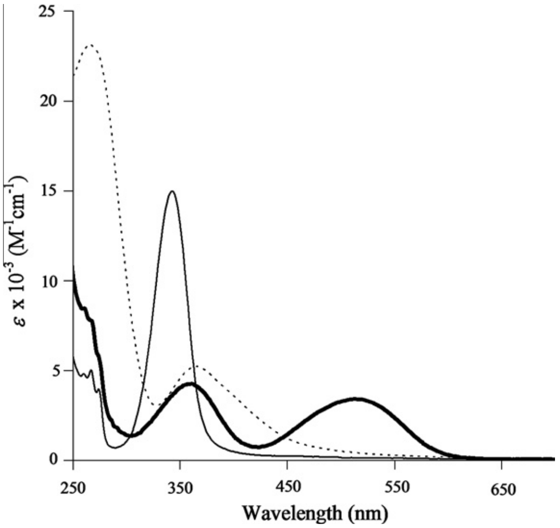

Fig. 9. Electronic absorption spectra: $[BzPh_3P][\mathbf{1}]$ in MeOH (—), **2** in CH_2Cl_2 (- - -) and $[BzPh_3P][\mathbf{4}]$ in THF (▬).

$[BzPh_3P][Cu(Br)(S\text{-}i\text{-}dto^tBu)]$ displays two broad and prominent bands at 358 nm (3730 M^{-1} cm^{-1}) and 512 nm (3420 M^{-1} cm^{-1}) with a low energy tailing at 720 nm (shoulder, 27 M^{-1} cm^{-1}). Notably, the spectra of $[BzPh_3P][\mathbf{4}]$ in different solvents exhibits solvatochromic behavior for the stronger bands as summarized in Table 7.

The lowest lying singlet electronic excited states of **4** and its theoretical electronic absorption spectrum were calculated using time-dependent DFT at the B3LYP/6-31G* level. This TD-DFT calculation predicted the absorption bands at 646 nm [(HOMO-1, 83%) → LUMO, or XLCT (where X is Br and L is the perthiocarboxylate ligand, and CT is charge transfer)]; at 499 nm [(HOMO-5, 89%) → LUMO, or largely MLCT]; overlapping transitions at 426 nm [(HOMO-3, 65%) → LUMO, largely σ_{CuBr} to $\pi_L{}^*$ CT] and at 409 nm [(HOMO-6, 89%) → LUMO, or $\pi_L \rightarrow \pi_L{}^*$ ligand localized]; and 356 nm [(HOMO-7, 68%) → LUMO, or largely $d_{Cu},\sigma_L \rightarrow \pi_L{}^*$]. Fig. 10 is the DFT predicted electronic absorption spectrum of $[BzPh_3P][\mathbf{4}]$ (in vacuum) overlaid with the experimental spectrum measured in CH_2Cl_2. The strongest transitions in the electronic absorption spectrum are predicted to be at about 356 and ca. 426 nm, respectively (in vacuum) and the calculated oscillator strengths (f^{calc}) of these are less than factor of two larger than the experimental f^{exp} values calculated from the product of ε_{max} and the full width at half maximum (in cm^{-1}).

Several mechanisms can be considered for the observed solvatochromism for **4** described in Table 7 [33–35]. Experimentally, the relative position of the two prominent bands ($\nu_{max}{}^{UV} - \nu_{max}{}^{Vis} \sim 8.5 \times 10^3$ cm^{-1}) is similar in each solvent so this agues against any major structural change from one medium to another.

Table 7
Effect of solvent on the electronic absorption spectrum of $[BzPh_3P][Cu(Br)(S\text{-}i\text{-}dto^tBu)]$.

Solvent	λ_{max} (nm)	λ_{max} (nm)	$\Delta\nu_{max}$ (cm^{-1})[a]	Rel. Abs[b]	ε[c]	π^*[d]	DN[e]
THF	513	358	8400	1.26	7.5	0.58	20
Acetone	508	357	8300	1.18	21	0.71	17
CH_2Cl_2	505	351	8700	1.06	9.1	0.82	0
MeCN	470	336	8500	0.89	37.5	0.75	14.1

[a] The difference in maximal frequency between ultraviolet and visible bands in each solvent.

[b] A^{UV}/A^{Vis}.

[c] Solvent dielectric constant.

[d] Kamlet solvent polarity factor [34].

[e] Solvent donor number from Linert et al. [33].

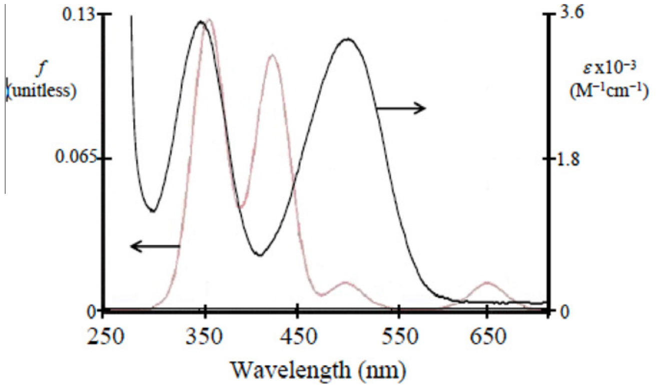

Fig. 10. TD-DFT calculated (B3LYP/6-31*, in vacuum, —) and experimental (in CH_2Cl_2, —) electronic absorption spectrum of **4**. The spectra are artificially normalized based on the appropriate vertical scale (f = oscillator strength for the calculated spectrum and ε = experimental extinction coefficient).

Furthermore the shifts did not correlate with the solvent donor numbers, so it appears that the anion **4** may remain 3-coordinate in solution. In this context ESI-MS experiments in both THF or MeCN gave $[Cu(Br)(S\text{-}i\text{-dto}^tBu)]^-$ as the major ion with no evidence of solvent adducts. From the DFT calculations we should expect the two strongest transitions to have similar character, both having significant MLCT contributions, thus similar dipolar changes between the ground and excited states.

In summary, we describe here the synthesis, structures and some properties of the ligand *O*-*t*-butyl-1,1-dithiooxalate, $i\text{-dto}^tBu^-$ and of bidentate and a monodentate complexes of this ligand with copper(I). In an attempt prepare a photochemically active Cu(II) complex of this ligand, we found that the reaction of **1** with $CuBr_2$ gave a deep red, crystalline Cu(I) compound, $[BzPh_3P]$[**4**], instead of the expected $Cu(i\text{-dto}^tBu)_2$. The structure of **4** showed the copper to be 3-coordinate and planar with a bidentate perthio-1-thiooxalato ligand $S\text{-}i\text{-dto}^tBu^-$, apparently the product of the disproportionation of **1** as has been described previously [4]. The S–S bond of the CuSSC=S cycle proved to be quite short, suggesting delocalization of the disulfide sulfur lone pairs. Data from mass spectrometry and the electronic absorption spectroscopy in various solutions of **4**, indicate that solvent is not strongly bound (if at all).

Acknowledgements

The authors thank Dr. James Pavlovich (UCSB) for helpful discussions on mass spectrometry techniques and Dr. Megan Grabenauer (UCSB) for performing the nanospray MS experiments. This work was partially supported by a grant from the U.S. National Science Foundation (NSF – CHE-0749524).

Appendix A. Supplementary material

CCDC 807531–807534 contains the supplementary crystallographic data for this paper. These data can be obtained free of charge from The Cambridge Crystallographic Data Centre via www.ccdc.cam.ac.uk/data_request/cif.

Spectroscopic properties of complexes (Figs. S1–S9), Packing diagram for $[BzPh_3P][CuBr(S\text{-}i\text{-dto-O}^tBu]\cdot0.5THF$, Results of DFT calculations (two tables and one figure).

Supplementary data associated with this article can be found, in the online version, at doi:10.1016/j.ica.2011.02.037.

References

[1] P.C. Ford, Acc. Chem. Res. 41 (2008) 190.
[2] P. Strauch, B. Dempe, R. Kempe, W. Dietzsch, J. Sieler, E. Hoyer, Z. Anorg. Allg. Chem. 620 (1994) 498.
[3] J. Piotraschke, P. Strauch, G. Zahn, E. Hoyer, Z. Anorg. Allg. Chem. 620 (1994) 505.
[4] J. Piotraschke, P. Strauch, S. Abram, U. Abram, Z. Anorg. Allg. Chem. 620 (1994) 1659.
[5] J. Piotraschke, P. Strauch, R. Kimse, Z. Anorg. Allg. Chem. 621 (1995) 159.
[6] J. Piotraschke, P. Strauch, Inorg. Chem. Acta 236 (1995) 177.
[7] R. Mas-Ballesté, A. Guijarro, R. González-Prieto, Ó. Castillo, P.J. Sanz Miguel, F. Zamora, J. Chem. Soc., Dalton Trans. 39 (2010) 1511.
[8] S.D. Pringle, K. Giles, J.L. Wildgoose, J.P. Williams, S.E. Slade, K. Thalassinos, R.H. Bateman, M.T. Bowers, J.H. Scrivens, Int. J. Mass Spectrom. 261 (2007) 1.
[9] G.M. Sheldrick, Acta Crystallogr., Sect. A 64 (2008) 112.
[10] Spartan '08, Wavefunction, Inc., Irvine, CA, Methods documented in: Y. Shao, L.F. Molnar, Y. Jung, J. Kussmann, C. Ochsenfeld, S.T. Brown, A.T.B. Gilbert, L.V. Slipchenko, S.V. Levchenko, D.P. O'Neill, R.A. DiStasio Jr., R.C. Lochan, T. Wang, G.J.O. Beran, N.A. Besley, J.M. Herbert, C.Y. Lin, T. Van Voorhis, S.H. Chien, A. Sodt, R.P. Steele, V.A. Rassolov, P.E. Maslen, P.P. Korambath, R.D. Adamson, B. Austin, J. Baker, E.F.C. Byrd, H. Dachsel, R.J. Doerksen, A. Dreuw, B.D. Dunietz, A.D. Dutoi, T.R. Furlani, S.R. Gwaltney, A. Heyden, S. Hirata, C.-P. Hsu, G. Kedziora, R.Z. Khalliulin, P. Klunzinger, A.M. Lee, M.S. Lee, W.Z. Liang, I. Lotan, N. Nair, B. Peters, E.I. Proynov, P.A. Pieniazek, Y.M. Rhee, J. Ritchie, E. Rosta, C.D. Sherrill, A.C. Simmonett, J.E. Subotnik, H.L. Woodcock III, W. Zhang, A.T. Bell, A.K. Chakraborty, D.M. Chipman, F.J. Keil, A. Warshel, W.J. Hehre, H.F. Schaefer, J. Kong, A.I. Krylov, P.M.W. Gill, M. Head-Gordon, Phys. Chem. Chem. Phys. 8 (2006) 3172.
[11] O. Niyomura, Y. Kitoh, Sulfur Lett. 22 (1999) 195.
[12] R. Mattes, W. Meschede, Chem. Ber. 109 (1976) 1832.
[13] G.A. Bowmaker, N. Chaichit, J.V. Hanna, C. Pakawatchi, B.W. Skelton, A.H. White, J. Chem. Soc., Dalton Trans. 38 (2009) 8308.
[14] G.A. Jeffrey, R. Shiono, Acta Crystallogr. 12 (1959) 447.
[15] D. Coucouvanis, S.J. Lippard, J. Am. Chem. Soc. 91 (1969) 307.
[16] F. Mévellec, A. Roucoux, N. Noiret, H. Patin, F. Tisato, G. Bandoli, Inorg. Chem. Commun. 2 (1999) 230.
[17] F. Mévellec, F. Tisato, F. Refosco, A. Roucoux, N. Noiret, H. Patin, G. Bandoli, Inorg. Chem. 41 (2002) 598.
[18] A. Müller, M. Lemke, E. Krickemeyer, H. Bögge, M. Penk, Monatsh. Chem. 124 (1993) 857.
[19] A.H. Mahmoudkahni, V. Langer, Acta Cyrstallogr., Sect. E 57 (2001) m92.
[20] J.P. Fackler Jr., J.A. Fetchin, D.C. Fries, J. Am. Chem. Soc. 94 (1972) 7323.
[21] L.J. Maheu, L.H. Pignolet, Inorg. Chem. 18 (1979) 3626.
[22] D. Coucouvanis, S. Kanodia, D. Swenson, S.-J. Chen, T. Stüdemann, N.C. Baenziger, R. Pedelty, M. Chu, J. Am. Chem. Soc. 115 (1993) 11271.
[23] C.W. Liu, R.J. Staples, J.P. Fackler, Coord. Chem. Rev. 174 (1998) 147.
[24] G.W. Kutney, K. Turnbull, Chem. Rev. 82 (1982) 333.
[25] R. Steudel, Angew. Chem., Int. Ed. 14 (1975) 655.
[26] R.L. Kuczkowski, J. Am. Chem. Soc. 86 (1964) 3617.
[27] R. Steudel, Y. Drozdova, K. Miaskiewicz, R.H. Hertwig, W. Koch, J. Am. Chem. Soc. 119 (1997) 1990.
[28] R. Cea-Olivares, V. García-Montalvo, S. Hernández-Ortega, C. Rodríguez-Narvaez, P. García y García, M. López-Cardoso, P. de March, L. González, L. Elias, M. Figueredo, J. Font, Tetrahedron: Asymmetry 10 (1999) 3337–3340.
[29] Q.-H. Jin, X.-L. Xin, Acta Crystallogr., Sect. C 55 (1999). IUC9900107.
[30] C. Pettinari, G.G. Lobbia, G. Sclavi, D. Leonesi, Polyhedron 14 (1995) 1709.
[31] F.H. Jardine, A.G. Vohra, F.J. Young, J. Inorg. Nucl. Chem. 33 (1971) 2941.
[32] M.A. Bernard, M.-M. Borel, G. Dupriez, Rev. Chem. Miner. 12 (1975) 181.
[33] W. Linert, Y. Fukuda, A. Camard, Coord. Chem. Rev. 218 (2001) 113.
[34] M.J. Kamlet, J.-L.M. Abboud, M.H. Abraham, R.W. Taft, J. Org. Chem. 48 (1983) 2877.
[35] C. Reichardt, Chem. Rev. 94 (1994) 2319.